(Received 19 July 2024, Accepted 11 October 2024, Scheduled 21 October 2024)

A Multi-Channel Error Compensation Method for Space-Borne RDBF-SAR

Lu Bai[1,2,*], Wei Xu[1,2], Pingping Huang[1,2], Weixian Tan[1,2], and Yaolong Qi[1,2]

[1] College of Information Engineering, Inner Mongolia University of Technology, Hohhot, China
[2] Inner Mongolia Key Laboratory of Radar Technology and Application, Hohhot, China

ABSTRACT: The time-varying amplitude error and phase error in the multi-channel will affect the system performance of Range Digital Beam Forming-Synthetic Aperture Radar (RDBF-SAR), which will lead to the elevation of the side lobes amplitude of the echo signal, thus affecting the quality of space-borne synthetic aperture radar (SAR) images. A multi-channel error compensation method for space-borne RDBF-SAR is proposed in this paper. The echo signals of each channel are aligned in the frequency domain. For the amplitude error, the amplitude error compensation factor is obtained by comparing the amplitude of each channel signal with the amplitude of the reference channel signal. For the phase error, the phase error compensation factor is obtained by conjugate multiplication of the phase of each channel signal and the phase of the reference channel signal. Reduce the amount of calculation by averaging. This method can well compensate the amplitude error and phase error, suppress the elevation of the echo side lobe, and make the synthetic aperture radar image more focused and accurate. Finally, the effectiveness of the method is verified by simulation experiments. Under the simulation conditions in this paper, the amplitude compensation reduces the side lobes pulse compression amplitude by $2 \sim 10$ dB, and the phase compensation reduces it by $-1 \sim 9$ dB.

1. INTRODUCTION

Space-borne synthetic aperture radar (SAR) technology uses microwave radiation for remote sensing imaging, which is not affected by weather, light, and clouds. It can perform target reconnaissance, disaster monitoring, resource exploration, and other tasks in various complex environments, and plays a vital role in military and civilian fields. However, the traditional single-channel space-borne SAR is limited by the minimum antenna area [1], which cannot meet the imaging requirements of wide swath while meeting the high-resolution imaging. The space-borne SAR range multi-channel system divides the receiving antenna panel into several sub-antennas along the range direction, and the wide beam covering the entire mapping area is transmitted by the transmitting channel. The receiving end receives multiple echoes from the mapping band through multiple sub-channels [1]. Digital beamforming (DBF) technology can suppress interference signals from other directions at the same time and frequency, so as to form a high-gain pencil beam in a specific direction and track the echo in real time [2]. Space-borne SAR range multi-channel system combined with DBF technology [3–6] can achieve high resolution wide swath imaging.

However, due to differences in manufacturing processes and processing environments, channel errors inevitably exist between the channels of the range multi-channel system, which will affect the identification and quantitative analysis of the target, resulting in SAR image blurring, thereby reducing the performance of DBF [1]. Therefore, it is necessary to compensate or calibrate the amplitude and phase errors between the channels of the multi-channel system [7–10]. In view of the above problems, scholars have carried out in-depth research on distance multi-channel and DBF technology [11–17]. In 2016, a DBF method suitable for multi-channel signal registration and merging was proposed [18]. In 2019, an algorithm that can effectively estimate the weight coefficient of DBF between channels was proposed, and the computational complexity was reduced [19]. In 2021, a novel weight generator and an improved DBF real-time processing architecture were proposed. The proposed generator can well correct the multi-channel amplitude and phase errors [20]. In 2024, an innovative method combining SAR imaging with DBF and multiple-input multiple-output (MIMO) technology was proposed. This method significantly reduces the computational time required for SAR image formation and has better phase error suppression ability [21].

The existing error compensation methods mentioned above generally do not consider the time-varying of amplitude and phase errors in order to simplify the calculation, but the amplitude and phase errors in the actual space-borne SAR range multi-channel system are more complicated. In the multi-channel DBF processing, each channel performs analog to digital (A/D) conversion and other operations independently, resulting in time-varying amplitude and phase errors. Based on the analysis of time-varying amplitude and phase errors, a multi-channel error compensation method for space-borne RDBF-SAR is proposed in this paper. Firstly, the echo signals of each distance channel corresponding to the same target point are aligned by translation. Then, the amplitude and phase error compensation factors of the other channels are calculated

* Corresponding author: Lu Bai (20221800100@imut.edu.cn).

by using the first channel as the reference channel. Through block average and weighted average methods, the calculation results are more accurate while reducing the amount of calculation, reducing the influence of local errors, and making the final imaging results clearer and more reliable.

The main sections of this paper are as follows. Section 2 introduces the principle of RDBF-SAR processing. Section 3 analyzes the influence of amplitude and phase errors on RDBF-SAR. Section 4 proposes a multi-channel error compensation method for space-borne RDBF-SAR. Section 5 is simulation verification. Finally, Section 6 summarizes the full text.

2. MULTI-CHANNEL RDBF-SAR PROCESSING

As shown in Figure 1, the multi-channel DBF working geometric model of space-borne SAR in range direction at a certain azimuth time is shown. In this paper, a "one transmitter and multiple receivers" system in the range direction is studied. Channel 1 is used as a reference channel to transmit a linear frequency modulation signal. There are a total of K receiving channels in the range direction to receive SAR echo. The distance between adjacent receiving channels is equal and is represented by d. H represents the satellite height. Any point P in the imaging scene is used as the reference point target. Assuming that the transmitting beam passes through the point target P, the beam center of the DBF points to the point P exactly. The distance from the point target P to the reference channel is denoted by R_0. α is the angle between the normal and vertical directions of the antenna. β_0 is the angle of view of point target P, that is, the angle between the oblique distance of P point and the vertical direction. P_1 and P_2 are two distance fuzzy points around P point. β_1 and β_2 are the perspectives of P_1 and P_2, respectively.

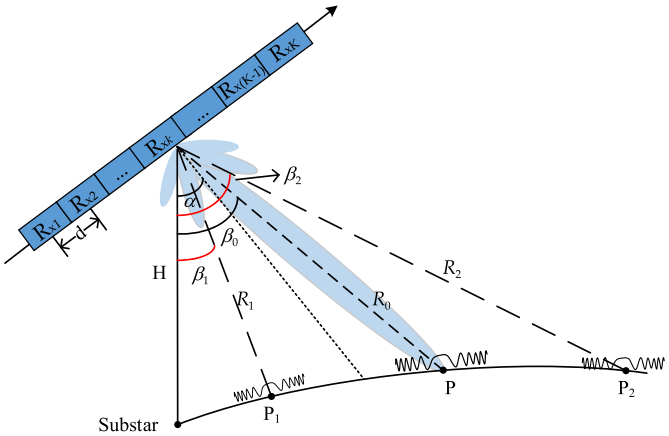

FIGURE 1. DBF schematic diagram of space-borne SAR range multi-channel.

The baseband echo signal of the point target P received by the kth $(k = 1, 2, ..., K)$ channel can be expressed as follows [4]:

$$\begin{aligned} \mathbf{s}_k(\tau) &= \text{rect}\left[\frac{\tau - 2R_0/c + \Delta\tau_k}{T_r}\right] \\ &\times \exp\left(-j2\pi f\left(2R_0/c - \Delta\tau_k\right)\right) \\ &\times \exp\left(j\pi k_r\left(\tau - 2R_0/c + \Delta\tau_k\right)^2\right) \end{aligned} \quad (1)$$

where $\Delta\tau_k$ denotes the delay between the return echo from P point arriving at the reference channel and that arriving at the kth channel.

$$\Delta\tau_k = \frac{(k-1)\,d\cdot\sin(\beta_0 - \alpha)}{c} \quad (2)$$

$$\beta_0 = \arccos\left[\frac{(H+R_e)^2 - R_e^2 + R_0^2}{2(H+R_e)\cdot R_0}\right] \quad (3)$$

where R_e represents the radius of the earth.

Figure 2 is the DBF processing flowchart of the multi-channel SAR in the range direction. Each channel first passes through the low noise amplifier, and then performs down conversion and analog-to-digital conversion. Due to the time difference of the echo signal received by each channel, it is necessary to multiply the corresponding time-varying weighting coefficients for each channel and introduce time delay compensation, so that the echo signals of different channels have better coherence.

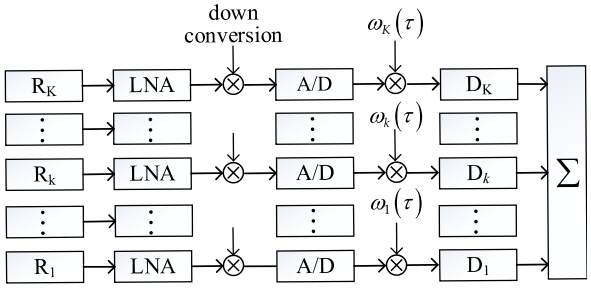

FIGURE 2. The DBF flowchart of range multi-channel SAR.

When time-varying weighting is performed on each channel in the distance direction, in order to make the center point of the formed receiving beam point to the center position of the pulse at all times, it is necessary to obtain the weighting coefficient of each channel according to the position of the pulse center [3]. The weighting coefficient of the kth channel can be expressed as:

$$\omega_k(\tau) = \exp\left(-j2\pi\frac{(k-1)\cdot d}{\lambda}\cdot\sin\left(\beta_k(\tau) - \alpha\right)\right) \quad (4)$$

where,

$$\beta_k(\tau) = \arccos\left[\frac{(H+R_e)^2 - R_e^2 + R_k(\tau)^2}{2(H+R_e)\cdot R_k(\tau)}\right] \quad (5)$$

where $\beta_k(\tau) - \alpha$ represents the normal shift angle of the center of the pulse, which varies with time. $R_k(\tau)$ represents the slant distance of the pulse center.

After time-varying weighting, it is also necessary to perform time delay processing on the time domain of the echo. The signal delay corresponding to the kth channel is:

$$D_k = \frac{k-1}{K_r}\cdot\frac{d}{\lambda}\cdot\left.\frac{\partial\theta(\tau)}{\partial\tau}\right|_{\tau=\tau_c} \quad (6)$$

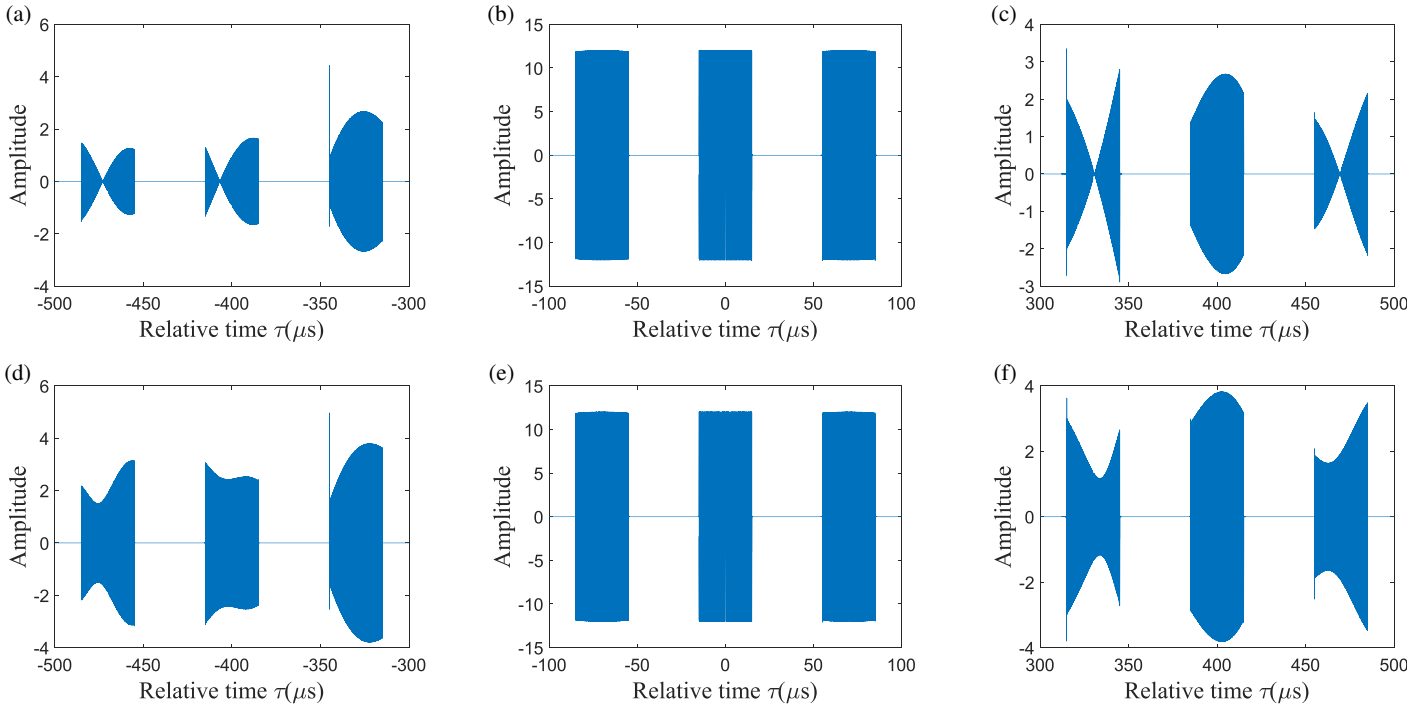

FIGURE 3. Comparison of echo signals before and after adding amplitude error: (a), (b), and (c) are the left side lobe, the main signal, and the right side lobe echo signal without amplitude error, respectively; (d), (e), and (f) are the left side lobe, the main signal, and the right side lobe echo signal with amplitude error, respectively.

where $\theta(\tau)$ is a time-varying perspective, and $\frac{\partial\theta(\tau)}{\partial\tau}\Big|_{\tau=\tau_c}$ in formula (6) is the first-order partial derivative of the function $\theta(\tau)$ with respect to the distance time variable τ in the center of the scene. τ_c is the distance time of the beam pointing to the center of the mapping strip.

In the above DBF processing, the influence of channel error is not considered. However, due to the differences in the receiver devices of each channel, the different working states, independent A/D conversion, and other operations, the signal of each channel inevitably has amplitude error and phase error.

3. THE INFLUENCE OF CHANNEL ERROR ON RDBF

Taking 12 receiving channels as an example, the influence of amplitude and phase errors on the range multi-channel DBF process of space-borne SAR is studied. The simulation is carried out by software MATLAB R2019b, and the built-in function of MATLAB is used to simulate the time-varying amplitude and phase noise. The system simulation parameters are shown in Table 1.

3.1. Amplitude Error

In the actual range multi-channel SAR system, a large part of the amplitude error between channels is due to the heat generated by the work of each channel receiver, which generally obeys the Gaussian distribution. We use the built-in function randn( ) in MATLAB software to generate random numbers with a mean of 0 and a variance of 1.5 that obey the Gaussian distribution to simulate the amplitude error of each channel.

TABLE 1. System simulation parameters.

Parameter	Symbol	Value (Unit)
Carrier frequency	f_0	9.6 GHz
Satellite altitude	H	675 km
Signal bandwidth	B_r	500 MHz
Pulse width	T_r	30 µs
Pulse-repetition frequency	PRF	2500 Hz
Number of channels	K	12
Adjacent channel spacing	d	0.3 m

Firstly, it is assumed that there is no amplitude error between channels. As shown in Figures 3(a), (b) and (c) show the echo images of the left side lobe echo signal, main signal, and right side lobe echo signal without amplitude error, respectively. The main lobe signal is usually reflected directly from the target back to the radar receiver, and the echo gain is high, as shown in Figure 3(b). The side lobe signal comes from the reflection of the target object in the side lobe region of the radar antenna, and the gain of the side lobe echo signal is low, as shown in Figures 3(a) and (c). Then, random numbers are added to each channel to simulate the amplitude error. When there is an amplitude error, the main lobe gain of the antenna pattern is basically unchanged. Therefore, the existence of amplitude error has little effect on the main echo signal, as shown in Figure 3(d). The existence of amplitude error will raise the pattern of the side lobe, so that the echo signal amplitude of the side lobe is raised by about 1–2 dB, as shown in Figures 3(e) and (f).

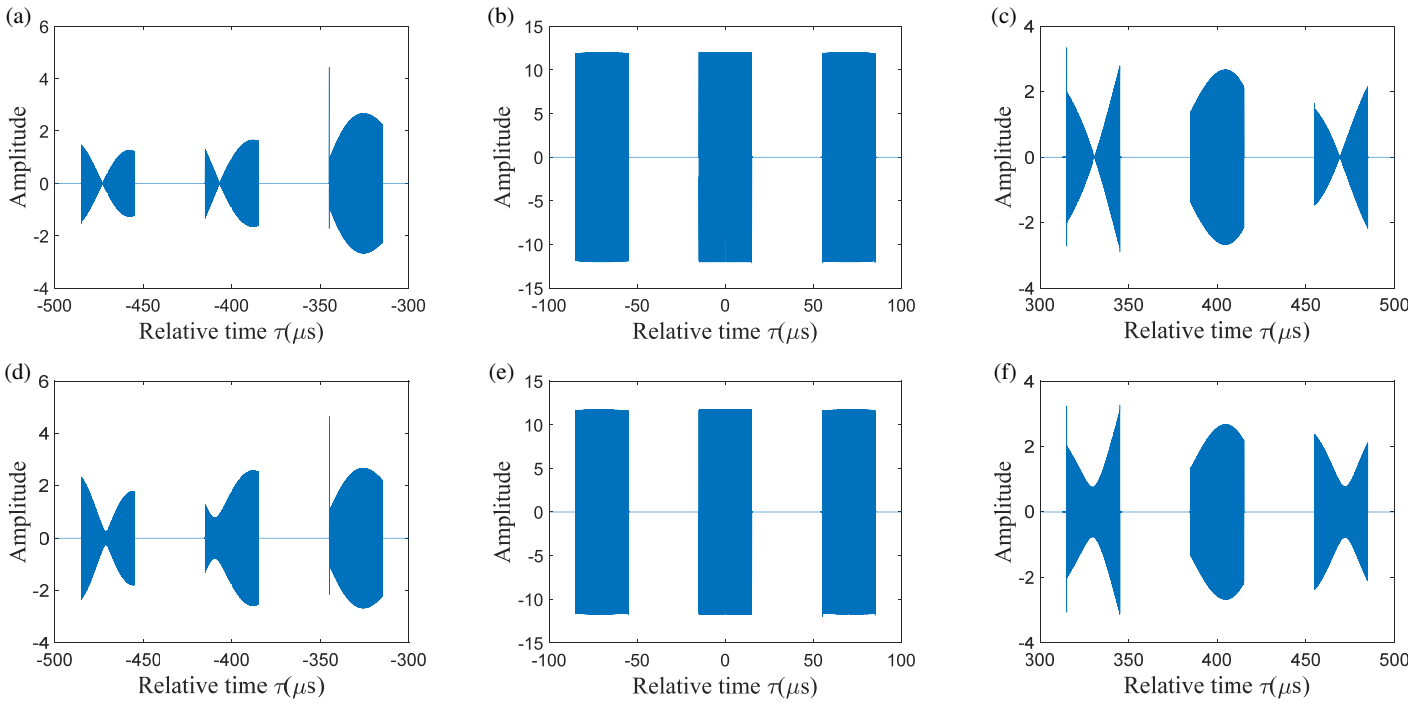

FIGURE 4. Comparison of echo signals before and after adding phase error: (a), (b), and (c) are the left side lobe, main signal, and right side lobe echo signal without phase error, respectively; (d), (e), and (f) are the left side lobe, main signal, and right side lobe echo signal with phase error, respectively.

3.2. Phase Error

The phase error between channels generally obeys uniform distribution. We use the built-in function unifrnd $(-10, 10)$ in MATLAB software to generate random numbers uniformly distributed from $-10°$ to $10°$ to simulate the phase error of each channel. Firstly, it is assumed that there is no phase error between channels. Figures 4(a), (b), and (c) are the echo patterns of the left side lobe echo signal, point target main signal, and right side lobe echo signal without phase error, respectively. Then, random numbers are added to each channel to simulate the phase error. Figures 4(d), (e), and (f) are the echo diagrams of the left side lobe echo signal, main signal of the point target, and right side lobe echo signal with phase error, respectively.

Similarly, the existence of phase noise has little effect on the main echo signal, but it increases the amplitude of the side lobe echo signal corresponding to the range ambiguity points on both sides of the point target. The sensitivity of the side lobe echo signal to the phase error is less than the amplitude error. The existence of the phase error will increase the amplitude of the side lobe echo signal by about 1 dB.

Due to the existence of amplitude and phase errors, the side lobe gain of echo signal will be increased, which will affect the range ambiguity suppression effect and further affect the quality of SAR image. Therefore, it is necessary to study the error compensation method for multi-channel DBF in the range direction of space-borne SAR.

4. ERROR COMPENSATION METHOD FOR SPACE-BORNE RDBF-SAR

In order to effectively suppress the range ambiguity and reduce the echo amplitude of the side lobes on both sides of the target point, we propose a multi-channel error compensation method for space-borne RDBF-SAR. Figure 5 shows the flowchart of error compensation method, which is divided into three parts. The first part is to shift and align the echo signals of each channel, the second part to compensate the amplitude error, and the third part to compensate the phase error.

The specific method flow is as follows.

4.1. Shift Alignment

1) Select the echo estimation region

As shown in Figure 6, the point with the largest signal-to-noise ratio (SNR) in the echo signal is selected as the P point. A section of echo signal near the P point is selected for the following operation. The region size is generally larger than a pulse width. $\Delta\tau$ is the time delay from the center edge of the transmitting pulse to the echo signal of P point.

2) Calculate the time delay of the region center

There is a certain delay τ_k in the P-point echo of each channel in the range direction. The delay of the kth channel is expressed as:

$$\tau_k = \Delta\tau_k + N \cdot \text{PRI} \tag{7}$$

where,

$$N = \left[\frac{2R_0}{c \cdot \text{PRF}}\right] \tag{8}$$

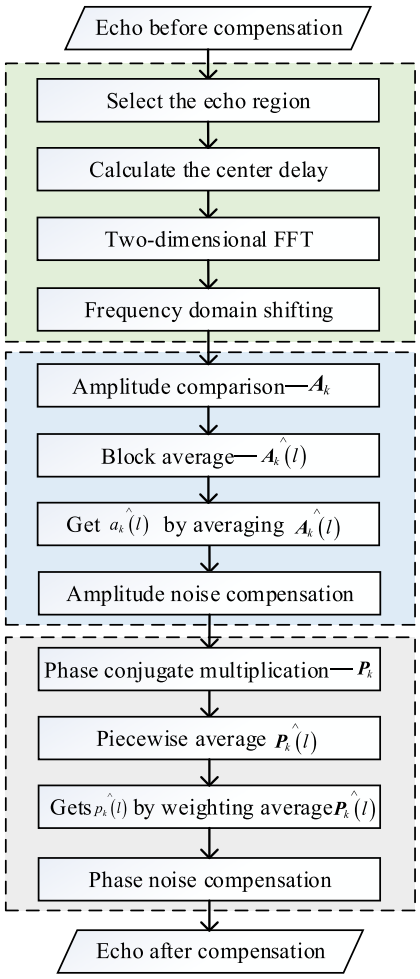

FIGURE 5. Flowchart of amplitude and phase noise compensation method.

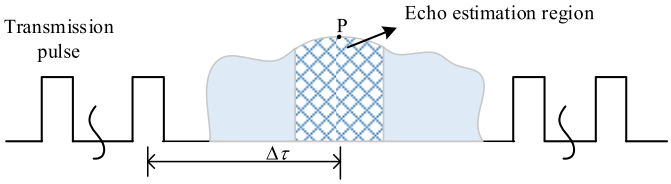

FIGURE 6. SAR echo signal schematic diagram.

where $[\cdot]$ denotes the downward rounding. PRI represents the pulse repetition interval.

3) The echo signal in the selected echo region is transformed to the frequency domain by fast Fourier Transform (FFT). The echo frequency domain signal of the kth channel is expressed as:

$$\mathbf{S}_k(f_r) = \mathrm{FFT}[\mathbf{s}_k(\tau)] \tag{9}$$

where $\mathrm{FFT}[\cdot]$ represents the Fourier transform.

4) The frequency domain echo signal of each channel is multiplied by the delay factor to realize the alignment of the echo pulses of each channel near the midpoint of the region. The expression of the frequency domain echoes of the kth channel multiplied by the delay factor is:

$$\mathbf{S}_k(f_r)' = \mathbf{S}_k(f_r)\exp(-j2\pi f\tau_k) \tag{10}$$

4.2. Amplitude Error Compensation

1) The amplitude of the echo signal of the kth channel after the shift alignment is compared with the amplitude of the echo signal of the reference channel, and the ratio is recorded as $\mathbf{A}_k$.

$$\begin{aligned}\mathbf{A}_{k[N_r\times N_a]} &= \frac{abs\left(\mathbf{S}_1(f_r)'\right)}{abs\left(\mathbf{S}_k(f_r)'\right)} \\ &= \begin{bmatrix} A_{1,1} & \cdots & A_{1,N_a} \\ \vdots & \ddots & \vdots \\ A_{N_r,1} & \cdots & A_{N_r,N_a} \end{bmatrix}\end{aligned} \tag{11}$$

where $abs(\cdot)$ represents the amplitude calculation of the signal. $\mathbf{A}_{k[N_r\times N_a]}$ represents that $\mathbf{A}_k$ is a $[N_r \times N_a]$ matrix. N_r is the number of frequency points in the range direction, and N_a is the number of sampling points in the azimuth direction.

2) In the azimuth direction, for any fixed distance frequency point, the amplitude error corresponding to each azimuth sampling point is different and fluctuates up and down. In order to compensate the amplitude error more accurately, we calculate the mean value for each n azimuth sampling points.

$$\hat{\mathbf{A}_k}(l) = \begin{bmatrix} \mathbf{E}\{\mathbf{A}_k[1,(l-1)n+1:\mathrm{ln}]\} \\ \mathbf{E}\{\mathbf{A}_k[2,(l-1)n+1:\mathrm{ln}]\} \\ \vdots \\ \mathbf{E}\{\mathbf{A}_k[\mathbf{N}_r,(l-1)n+1:\mathrm{ln}]\} \end{bmatrix}_{[\mathbf{N}_r,1]} \tag{12}$$

where $E\{\cdot\}$ represents the mean value operation, $l = 1,2,...,N_a-\omega+1$. ω is the remainder of the division of N_a and n. $(l-1)n+1:\mathrm{ln}$ represents the column $(l-1)n+1$ to column ln of $\mathbf{A}_k$.

3) Average $\hat{\mathbf{A}_k}(l)$ to get $\hat{a_k}(l)$.

$$\hat{a_k}(l) = E\left[\hat{\mathbf{A}_k}(l)\right] \tag{13}$$

4) Amplitude error compensation is performed by multiplying each channel signal by $\hat{a_k}(l)$.

$$\hat{\mathbf{S}_k}(l) = \hat{a_k}(l)\cdot\mathbf{S}_k(l)' \tag{14}$$

where,

$$\mathbf{S}_k(l)' = \mathbf{S}_k[:,(l-1)n+1:\mathrm{ln}]' \tag{15}$$

where $\hat{\mathbf{S}_k}(l)$ represents the partial echo signal of the kth channel after amplitude error compensation.

4.3. Phase Error Compensation

1) The phase of the echo signal of the kth channel is conjugate multiplied by the phase of the echo signal of the reference channel to obtain $\mathbf{P}_{k[N_r\times N_a]}$.

$$\mathbf{P}_{k[N_r\times N_a]} = \mathrm{angle}\left(\mathbf{S}_k(f_r)'\right)\cdot\mathrm{angle}\left(\mathbf{S}_1(f_r)'\right)^*$$

$$= \begin{bmatrix} P_{1,1} & \cdots & P_{1,N_a} \\ \vdots & \ddots & \vdots \\ P_{N_r,1} & \cdots & P_{N_r,N_a} \end{bmatrix} \tag{16}$$

where angle $(\cdot)$ represents the phase calculation of the signal. $(\cdot)^*$ denotes taking conjugate. $\mathbf{P}_{k[N_r \times N_a]}$ represents that $\mathbf{P}_k$ is a matrix of $[N_r \times N_a]$; N_r is the number of frequency points in the range direction; and N_a is the number of sampling points in the azimuth direction.

2) Similarly, in the process of phase noise compensation, we still use block average in the azimuth direction and take the mean value once per n azimuth sampling points.

$$\overset{\wedge}{\mathbf{P}_k}(l) = \begin{bmatrix} \mathbf{E}\{\mathbf{P}_k[1, (\hat{l}-1)\, n+1 : \ln]\} \\ \mathbf{E}\left\{\mathbf{P}_k\left[2, (l-1)n+1 : \ln\right]\right\} \\ \vdots \\ \mathbf{E}\left\{\mathbf{P}_k\left[\mathbf{N}_r, (l-1)n+1 : \ln\right]\right\} \end{bmatrix}_{[\mathbf{N}_r,1]} \tag{17}$$

3) The influence of the phase error near the center frequency point on the echo is generally greater than that of the frequency points on both sides. In order to filter out the influence of individual outliers on the overall phase error estimation, we first weight $\overset{\wedge}{\mathbf{P}_k}(l)$ through the window function and then average it. Here, the Kaiser window is selected, and the window function formula is:

$$W_k(f,F) = \frac{I_0\left(\beta\sqrt{1-\left(\frac{2f}{F}\right)^2}\right)}{I_0(\beta)}, \quad -\frac{F}{2} \le f < \frac{F}{2} \tag{18}$$

where β is an adjustable attenuation coefficient, I_0 the zero-order Bessel function, and F the length of the window.

4) The average of $\overset{\wedge}{\mathbf{P}_k}(l)$ after the window function is:

$$\overset{\wedge}{p_k}(l) = E\left[\overset{\wedge}{\mathbf{P}_k}(l)\right] \tag{19}$$

5) Phase error compensation is performed by multiplying each channel signal by $\overset{\wedge}{p_k}(l)$.

$$\overset{\wedge\wedge}{\mathbf{S}_k}(l) = \overset{\wedge}{p_k}(l) \cdot \overset{\wedge}{\mathbf{S}_k}(l) \tag{20}$$

where $\overset{\wedge\wedge}{\mathbf{S}_k}(l)$ represents the partial echo signal of the kth channel after amplitude error and phase error compensation.

5. SIMULATION VERIFICATION

5.1. Amplitude Compensation

The error compensation method proposed in this paper is used to compensate the amplitude error of each channel in the distance direction. Figure 7(a) shows the signal echo corresponding to the distance ambiguity point on the left side of the point target after the amplitude error compensation. Compared with the range ambiguity echo signal without amplitude error, the amplitude difference is only about 0.5 dB, and the compensation effect is good. Figure 7(b) is the comparison of pulse compression amplitudes before and after amplitude error compensation. It can be clearly seen from the intermediate pulse amplification that the error compensation method in this paper reduces the pulse compression amplitude of distance ambiguity by about 7 dB. Similarly, as shown in Figure 7(c), the signal echo corresponding to the range ambiguity point on the right side of the point target is also well compensated. It can be seen from Figure 7(d) that the pulse compression amplitude of the right distance ambiguity point decreases by about 4.5 dB after amplitude compensation by the proposed method.

The existing traditional range multi-channel amplitude and phase error compensation method compensates the amplitude error and phase error in each channel as fixed values. The following compares the effect of error compensation using the traditional method and the method proposed in this paper. As shown in Figure 8(a), the blue curve is the range-blurred pulse compression amplitude in the presence of amplitude error. The yellow curve is the pulse compression amplitude after error compensation by the traditional method. The red curve is the pulse compression amplitude after error compensation using the method proposed in this paper. Due to different positions of the range ambiguity in the side lobe, the amplitude of pulse compression fluctuates greatly. Compared with the traditional method, it can be clearly seen that the error compensation method proposed in this paper can reduce the pulse compression amplitude of the side lobe more effectively. Figure 8(b) shows the difference of pulse compression amplitudes before and after amplitude compensation by the traditional method and the proposed method. Using the traditional method, the pulse compression amplitude of the side lobe can be reduced by 2 dB to 7 dB, and basically below 5 dB. By using the proposed error compensation method, the pulse compression amplitude of the side lobe is reduced by 2 dB to 10 dB, and it is basically above 5 dB.

5.2. Phase Compensation

Figures 9(a) and (c) are the signal echoes corresponding to the range ambiguity points on the left and right sides of the point target after phase error compensation, respectively. Compared with the range ambiguity echo signal without phase error, the amplitude difference is only about 0.5 dB, and the compensation effect is good. Figures 9(b) and (d) are the comparison of the pulse compression amplitudes before and after the compensation of the distance ambiguity point amplitude error on the left and right sides of the point target. The error compensation

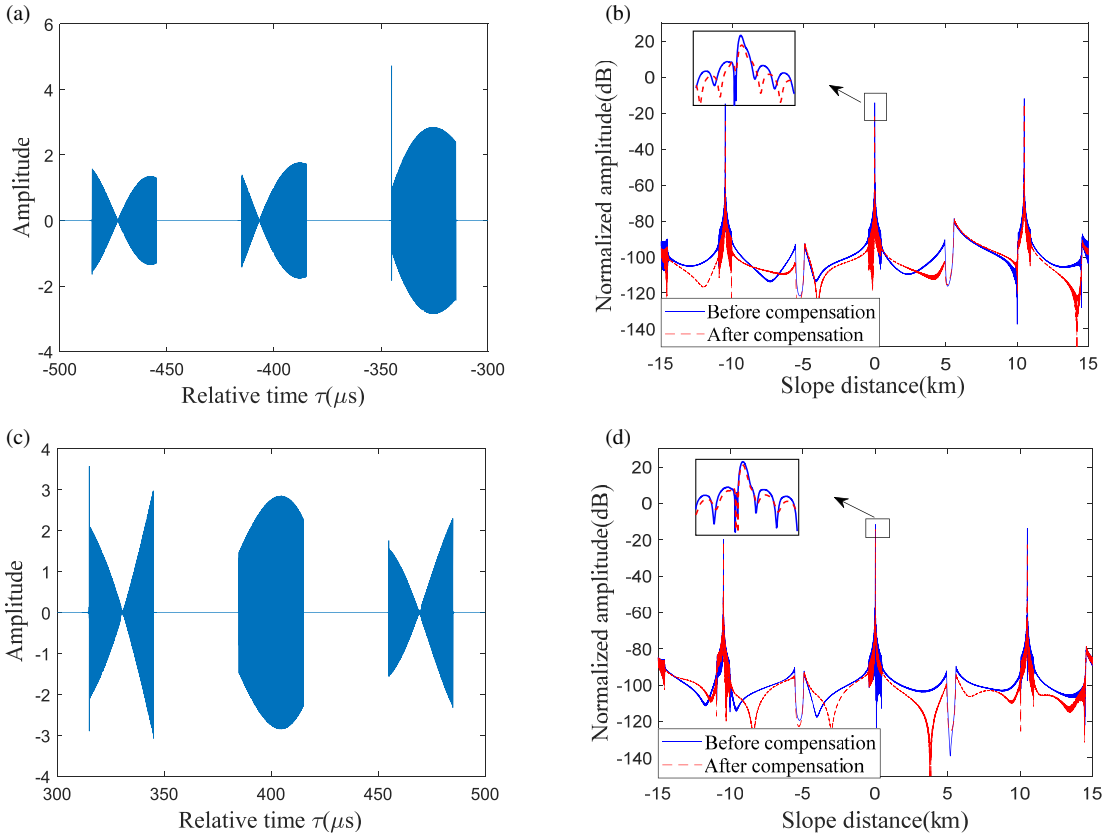

FIGURE 7. Range-ambiguous echo signal and pulse compression after amplitude error compensation: (a) and (c) are the echo signals of the left and right range ambiguity points respectively; (b) and (d) are the pulse compression before and after the amplitude error compensation of the left and right distance ambiguity points, respectively.

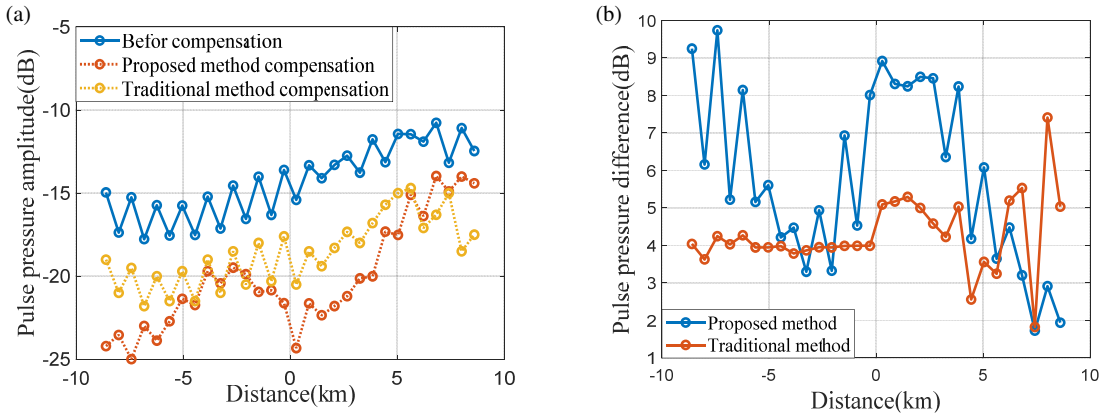

FIGURE 8. Comparison of pulse compression amplitude before and after amplitude error compensation: (a) pulse compression amplitude curve; (b) the amplitude difference curve of pulse compression before and after compensation.

method proposed in this paper improves the distance ambiguity and reduces the pulse compression amplitude.

As shown in Figure 10(a), the blue curve is the range-blurred pulse compression amplitude in the presence of phase error. The yellow curve is the pulse compression amplitude after error compensation by the traditional method. The red curve is the pulse compression amplitude after error compensation using the method proposed in this paper. Compared with the traditional method, it can be clearly seen that the error compensation method proposed in this paper can reduce the pulse compression amplitude of the side lobe more effectively. Figure 10(b) shows the difference of pulse compression amplitudes before and after amplitude compensation by the traditional method and the proposed method. Compared with the traditional error compensation method, the error compensation method proposed in this paper is more effective, and the pulse compression amplitude of the side lobe is reduced by $-1\,\mathrm{dB} \sim 9\,\mathrm{dB}$.

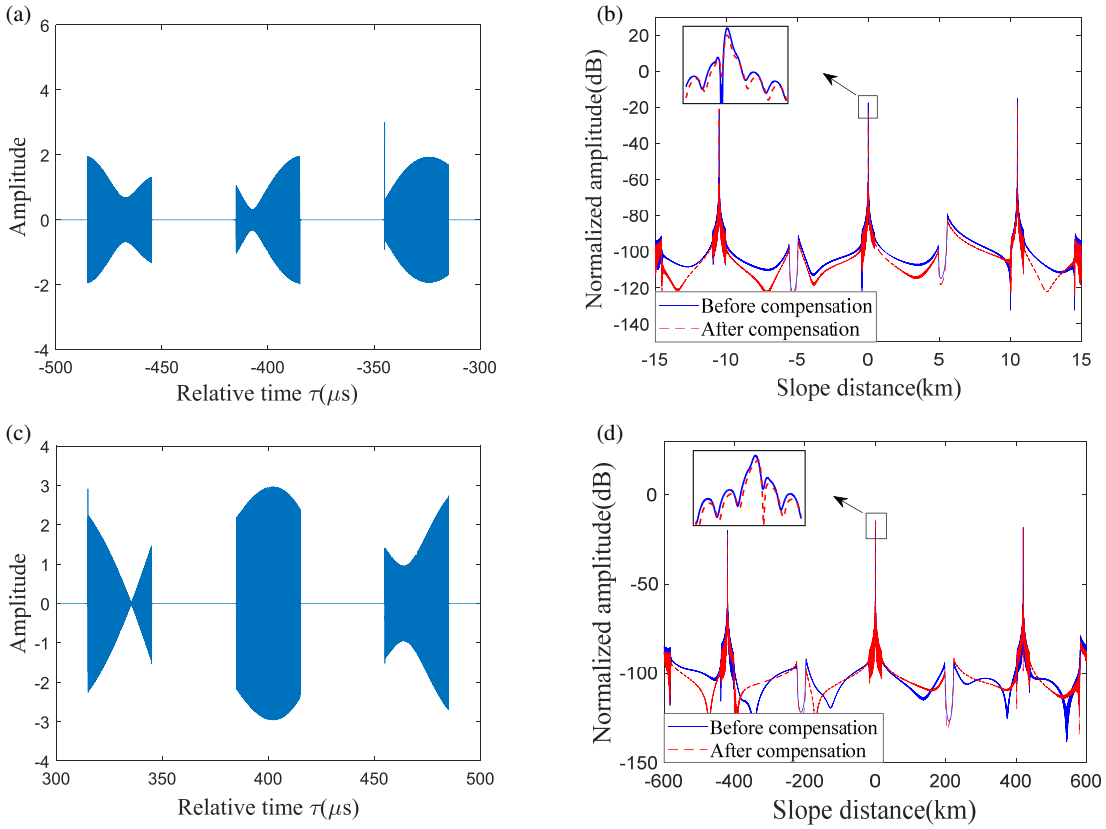

FIGURE 9. Range-ambiguous echo signal and pulse compression after phase error compensation: (a) and (c) are the echo signals of the left and right range ambiguity points respectively; (b) and (d) are the pulse compression before and after the phase error compensation of the left and right distance ambiguity points, respectively.

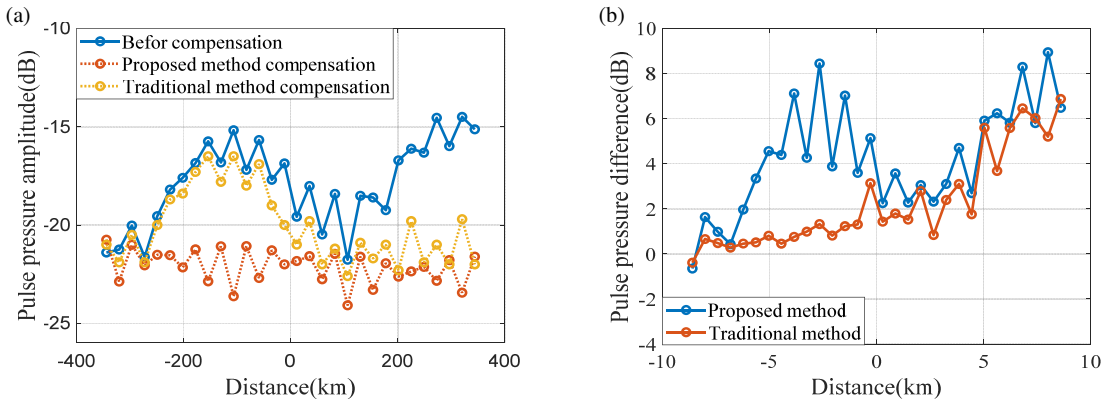

FIGURE 10. Comparison of pulse compression amplitude before and after phase error compensation: (a) pulse compression amplitude curve; (b) the amplitude difference curve of pulse compression before and after compensation.

5.3. Real Data Validation

In order to further verify the error compensation ability of the proposed algorithm in processing actual SAR data, this paper uses the X-band SAR real data collected by a domestic airborne radar to conduct experiments. The radar system has a signal bandwidth of 600 MHz, an antenna size of 0.32 m, and 8 channels in the range direction. Figure 11(a) shows the original SAR image of the main lobe in the range direction after DBF processing. Figure 11(b) shows the image compensated by the traditional distance error compensation method. Because the traditional error compensation method cannot compensate the amplitude and phase errors well, the amplitude of the side lobe echo is raised, and the SAR image is aliasing. Figure 11(c) is the SAR image compensated by the range error compensation method proposed in this paper. It can be seen that the channel error is compensated, the SAR image well focused, and the real scene basically restored.

Table 2 gives the amplitude and phase error data corresponding to different frequency points in the two channels of channel 2 and channel 4. The amplitude and phase errors corre-

TABLE 2. Error data of different frequency points.

		−300 MHz	−225 MHz	−150 MHz	−75 MHz	75 MHz	150 MHz	225 MHz	300 MHz
Amplitude	**Ch2**	4.54 dB	5.13 dB	4.80 dB	3.67 dB	4.32 dB	3.14 dB	4.97 dB	2.74 dB
	Ch4	−3.20 dB	−3.22 dB	−1.05 dB	−2.08 dB	−0.67 dB	−0.78 dB	−1.99 dB	−3.68 dB
Phase	**Ch2**	−21.46°	−23.74°	−22.55°	−25.23°	−20.82°	−23.07°	−24.11°	−25.20°
	Ch4	14.62°	16.78°	13.47°	12.20°	12.16°	15.98°	14.65°	14.61°

TABLE 3. Eight-channels error data.

	Ch1	Ch2	Ch3	Ch4	Ch5	Ch6	Ch7	Ch8
Mean of actual amplitude error	0 dB	4.16 dB	2.43 dB	−2.08 dB	3.59 dB	−2.24 dB	−4.92 dB	3.62 dB
Amplitude error estimation	0 dB	3.68 dB	2.95 dB	−1.89 dB	2.63 dB	−2.58 dB	−4.17 dB	2.57 B
Mean of actual phase error	0°	−23.27°	−9.35°	14.31°	−18.39°	4.62°	21.72°	19.64°
Phase error estimation	0°	−21.65°	−8.48°	12.71°	−19.83°	4.13°	20.34°	19.95°

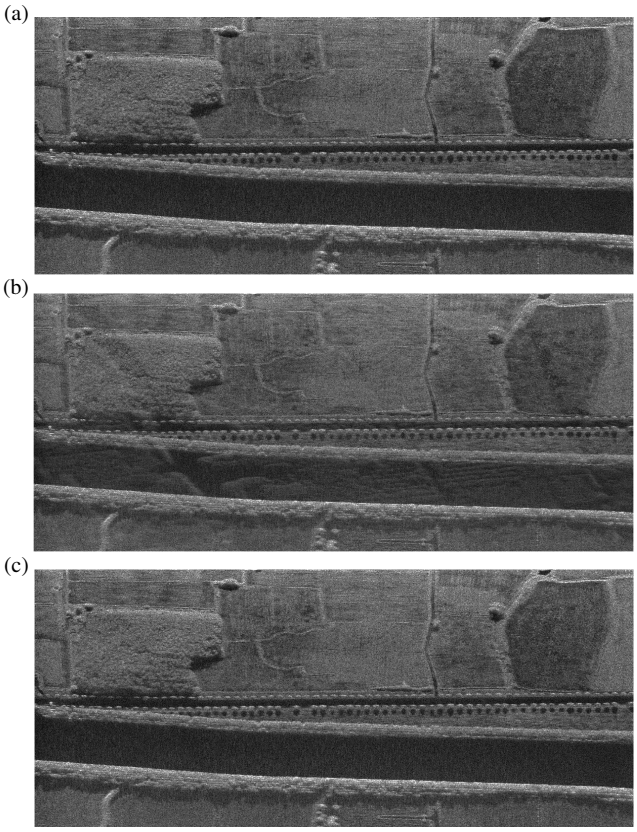

FIGURE 11. Comparison of imaging results of distributed targets: (a) original SAR image for simulation; (b) image after error compensation by traditional method; (c) image after error compensation by the proposed method.

sponding to each frequency point are different, so the method proposed in this paper compensates the amplitude and phase errors of each channel by calculating the mean value. Through calculation, the mean amplitude error in channel 2 is 4.16 dB, and the variance is 0.78. The mean amplitude error in channel 4 is −2.08 dB, and the variance is 1.40. The mean phase error in channel 2 is −23.27°, and the variance is 2.62. The mean phase error in channel 4 is 14.31°, and the variance is 2.71.

Since the amplitude and phase errors in each channel are time-varying, in order to facilitate comparison, we take the mean value of the actual amplitude and phase error data in each channel. Table 3 shows the data mean values of amplitude and phase errors in each channel and compares them with the error estimation results obtained by the proposed method. It can be seen that the amplitude estimation difference is less than 1 dB, and the phase estimation difference is less than 1.5°. The proposed method can effectively compensate the amplitude and phase errors.

6. CONCLUSION

In a space-borne SAR range multi-channel system, there are time-varying amplitude errors and phase errors between channels. The existence of these channel errors will affect the performance of multi-channel DBF in the range direction, resulting in the elevation of the side lobes amplitude of the echo signal and the generation of range ambiguity, thus affecting the quality of space-borne SAR images. In view of the above problems, this paper proposes an error compensation method for space-borne SAR range multi-channel DBF processing. Firstly, the echo estimation region is determined according to the point with the largest signal-to-noise ratio in the echo, and the time delay of the center of the region is calculated. The delay between the channels corresponding to the midpoint of the region is compensated by shift alignment. Then, the amplitude of the echo signal of each channel after the shift alignment is compared with the amplitude of the echo signal of the reference channel, and the ratio is averaged as the amplitude noise compensation factor. The phase compensation factor is obtained by conjugate multiplication of the phase of each channel echo signal and the phase of the reference channel, and the average is used to compensate the phase error. Due to the difference in the amplitude and phase errors corresponding to each sampling point in the azimuth direction, we use a block averaging method

for averaging azimuth sampling points. Finally, the simulation results show that the range ambiguity can be suppressed, and the side lobes amplitude can be reduced by using the amplitude and phase error compensation method proposed in this paper, so that the SAR image is clearer.

The amplitude and phase error compensation method proposed in this paper greatly suppresses the influence of channel error on distance ambiguity, but there are still some shortcomings. In particular, because the error of each n azimuth sampling point needs to be averaged once, the real-time performance of error compensation is limited. In order to overcome this problem, subsequent research such as adaptive algorithms can be added to improve computational efficiency without reducing computational accuracy, thereby achieving real-time error compensation.

REFERENCES

[1] Freeman, A., W. T. K. Johnson, B. Huneycutt, R. Jordan, S. Hensley, P. Siqueira, and J. Curlander, "The "Myth" of the minimum SAR antenna area constraint," *IEEE Transactions on Geoscience and Remote Sensing*, Vol. 38, No. 1, 320–324, 2000.

[2] Wang, Z., "Study on imaging techniques for spaceborne multichannel SAR/InSAR," Ph.D. dissertation, Xidian University, Xi'an, China, 2018.

[3] Li, B., Q. Zhao, Y. Zhang, D. Liang, W. Wang, Y. Cai, J. Li, P. Lu, and R. Wang, "An advanced sparse multi-channel system for spaceborne DBF-SAR," *IEEE Transactions on Geoscience and Remote Sensing*, Vol. 61, 5211513, 2023.

[4] Yu, Q., W. Xu, P. Huang, W. Tan, and Y. Qi, "An improved null steering digital beamformer based on multi-group time delays for echo separation in HRWS SAR," *Remote Sensing Letters*, Vol. 14, No. 6, 641–648, 2023.

[5] Xu, W., Q. Yu, C. Fang, P. Huang, W. Tan, and Y. Qi, "Onboard digital beamformer with multi-frequency and multi-group time delays for high-resolution wide-swath SAR," *Remote Sensing*, Vol. 13, No. 21, 4354, 2021.

[6] Yu, Q., J. Hu, H. Bi, W. Xu, P. Huang, and W. Tan, "Spaceborne real time DBF processing based on multi-group time delayers," *Journal of Signal Processing*, Vol. 38, 562–570, 2022.

[7] Chen, Z., Z. Zhang, J. Qiu, Y. Zhou, W. Wang, H. Fan, and R. Wang, "A novel motion compensation scheme for 2-D multichannel SAR systems with quaternion posture calculation," *IEEE Transactions on Geoscience and Remote Sensing*, Vol. 59, No. 11, 9350–9360, 2020.

[8] Pan, J., S. Wang, D. Li, and X. Lu, "A channel phase error compensation method for space borne array SAR based on antenna pattern and doppler correlation coefficient," *Journal of Electronics & Information Technology*, Vol. 41, No. 7, 1758–1765, 2019.

[9] Suo, Z., J. Ti, H. Xiang, L. Zhang, C. Xing, and T. Wang, "Airborne elevation DBF-TOPS SAR/InSAR method based on LOS motion compensation and channel error equalization," *Remote Sensing*, Vol. 14, No. 18, 4542, 2022.

[10] Wang, S., M. Xiang, B. Wang, F. Zhang, and Y. Wu, "A channel phase error compensation method for multi-channel synthetic aperture ladar," *Optik*, Vol. 178, 830–840, 2019.

[11] Yu, Q., "Research on digital beamforming in range of spaceborne SAR and its application," Ph.D. dissertation, Inner Mongolia University of Technology, Hohhot, Inner Mongolia, China, 2022.

[12] Li, B., "Study on elevation/azimuth multichannel SAR imaging," Ph.D. dissertation, Xidian University, Xi'an, China, 2021.

[13] Zhao, Q., Y. Zhang, W. Wang, K. Liu, Y. Deng, H. Zhang, Y. Wang, Y. Zhou, and R. Wang, "On the frequency dispersion in DBF SAR and digital scalloped beamforming," *IEEE Transactions on Geoscience and Remote Sensing*, Vol. 58, No. 5, 3619–3632, 2020.

[14] Huang, H., P. Huang, Y. Liu, H. Fan, Y. Deng, X. Liu, and G. Liao, "A novel method for staggered SAR imaging in an elevation multichannel system," *IEEE Transactions on Geoscience and Remote Sensing*, Vol. 61, 1–19, 2023.

[15] Younis, M., T. Rommel, F. Bordoni, G. Krieger, and A. Moreira, "On the pulse extension loss in digital beamforming SAR," *IEEE Geoscience and Remote Sensing Letters*, Vol. 12, No. 7, 1436–1440, 2015.

[16] Huber, S., M. Younis, G. Krieger, and A. Moreira, "Error analysis for digital beamforming synthetic aperture radars: A comparison of phased array and array-fed reflector systems," *IEEE Transactions on Geoscience and Remote Sensing*, Vol. 59, No. 8, 6314–6322, 2021.

[17] Han, S., Y. Deng, Q. Zhao, Y. Zhang, Y. Zhang, and W. Wang, "On spaceborne DBF-SAR adopting the degree of freedom with NLFM waveform: Optimization framework and simulation," *IEEE Transactions on Geoscience and Remote Sensing*, Vol. 60, 1–15, 2022.

[18] Wang, W., R. Wang, Y. Deng, W. Xu, and L. Hou, "Improved digital beam-forming approach with scaling function for range multi-channel synthetic aperture radar system," *IET Radar, Sonar & Navigation*, Vol. 10, No. 2, 379–385, 2016.

[19] Lei, W., D. Xu, H. Yu, and Y. Liu, "A study on adaptive SCORE processing for range DBF-SAR," *Modern Radar*, Vol. 41, No. 9, 37–40, 2019.

[20] Qiu, J., Z. Zhang, R. Wang, P. Wang, H. Zhang, J. Du, W. Wang, Z. Chen, Y. Zhou, H. Jia, and H. Sun, "A novel weight generator in real-time processing architecture of DBF-SAR," *IEEE Transactions on Geoscience and Remote Sensing*, Vol. 60, 1–15, 2021.

[21] Farhadi, M., R. Feger, J. Fink, T. Wagner, and A. Stelzer, "Combining MIMO DBF with automotive synthetic aperture radar imaging and phase error correction," *IEEE Access*, Vol. 12, 31 944–31 959, 2024.